

Article

Landslide Displacement Prediction Based on CEEMDAN Method and CNN–BiLSTM Model

Zian Lin ¹, Yuanfa Ji ² and Xiyan Sun ^{2,*}

¹ School of Computer Science and Information Security, Guilin University of Electronic Technology, Guilin 541004, China; 20031102010@mails.guet.edu.cn

² Information and Communication School, Guilin University of Electronic Technology, Guilin 541004, China; jiyuanfa@guet.edu.cn

* Correspondence: sunxiyan@guet.edu.cn

Abstract: Landslides are a typical geological disaster, and are a great challenge to land use management. However, the traditional landslide displacement model has the defect of ignoring random displacement. In order to solve this situation, this paper proposes a CNN–BiLSTM model that combines a convolutional neural network (CNN) model and a bidirectional long short-term memory network (BiLSTM) model. In this model, the CEEMDAN method is innovatively proposed to decompose landslide displacement. The GRA–MIC fusion correlation calculation method is used to select the factors influencing landslide displacement, and finally the CNN–BiLSTM model is used for prediction. The CNN–BiLSTM model was constructed to extract the temporal and spatial characteristics of data for landslide displacement prediction. Two new concepts that evaluate the state of a landslide and the trend of the landslide are proposed to improve the performance of the prediction model. Then, we discuss the prediction performance of the CNN–BiLSTM model under four different input conditions and compare it with seven other prediction models. The experimental prediction results show that the model proposed in this paper can be popularized and applied in areas with frequent landslides, and provide strong support for disaster prevention and reduction and land use management.

Keywords: land use management; landslide displacement prediction; complete ensemble empirical mode decomposition with adaptive noise; bidirectional long short-term memory



Citation: Lin, Z.; Ji, Y.; Sun, X.

Landslide Displacement Prediction Based on CEEMDAN Method and CNN–BiLSTM Model. *Sustainability* **2023**, *15*, 10071. <https://doi.org/10.3390/su151310071>

Academic Editors: Lu Zhang, Bing Kuang and Bohan Yang

Received: 6 June 2023

Revised: 22 June 2023

Accepted: 23 June 2023

Published: 25 June 2023



Copyright: © 2023 by the authors. Licensee MDPI, Basel, Switzerland. This article is an open access article distributed under the terms and conditions of the Creative Commons Attribution (CC BY) license (<https://creativecommons.org/licenses/by/4.0/>).

1. Introduction

As the seasons change, the weather warms, human activity expands, and the frequency of natural disasters increases [1]. All kinds of natural disasters, such as soil erosion, floods, volcanic eruptions, earthquakes, and tsunamis, among which landslides are the most destructive and harmful [2], can lead to the severe loss of lives and properties [3–5]. Landslides are geomorphological processes that involve the mobilization of the ground, rocks, debris, and the mud downslope under the action of gravity, causing local erosion problems [6,7]. Human disturbance is also an important triggering mechanism for landslides [8]. In most countries, landslides have caused severe socioeconomic impacts on people, cities, industrial establishments, and lifelines, including highways, railways, and communication network systems [9]. China is among the countries most vulnerable to landslides worldwide [10]. According to China's 2020 China Statistical Yearbook, 4810 landslides occurred in China in 2020, accounting for 61.3 percent of the country's total geological disasters, causing many property losses and casualties [11]. Therefore, it is important to obtain predictions and alerts for landslides, considering their causes and probability of occurrence, to issue timely landslide hazard warnings and prevent similar tragedies [12]. This also plays an important role in the policymaking of land use management.

Over the years, the field of landslide displacement prediction has benefited from the continuous development of artificial intelligence and landslide monitoring technologies. A

variety of analytical methods and machine learning models have been used for landslide displacement prediction [13–24]. Chenhui et al. [13] combined a genetic algorithm with the Elman neural network, optimized the weight, threshold, and number of hidden neurons of the Elman neural network, and solved the problem which Elman easily falls into, of local minima and neuron data being difficult to determine. Yong et al. [14] fused the predicted trend series with the sensitivity state to obtain the nonlinear prediction model. S.H. et al. [15] constructed a weighted multi-kernel grey model based on grey theory, multi-kernel learning and weighted learning. Lizhou et al. [16] proposed a nonlinear grey prediction model with background value optimization (BNGM(1, 1, t₂)) and compared it with three kinds of grey Bernoulli models, illustrating the advantages of the proposed model. Yanan et al. [17] proposed a new graph convolution network fused with the GRU model (GC-GRU-N) and applied it to landslide displacement prediction. Cheng et al. [18] improved the bootstrap method, used partial neural networks to construct PI, and used a random vector functional link network (RVFLN) instead of ELM as the predictor of the neural network. As a result, excellent landslide displacement interval prediction was achieved. Jingjing et al. [19] proposed the multi-feature fusion transfer learning (MFTL) method, utilizing the knowledge and skills gained from the Baijiapu landslide scenario, to improve the prediction ability of other landslides. Peihong et al. [20] considered the Laowuji landslide to be a research object, studied its dynamic failure mode, and finally decided to use a variety of factors, including geological conditions, rainfall intensity and human activities, as input and used a long short-term memory (LSTM) model to predict landslide displacement. Heming et al. [21] recombined the mutation displacement data to reduce the displacement of the mutation-affected data in the steady state and accurately predicted the displacement of the landslide mutation segment. Shaohong et al. [22] combined dual support vector regression with the Hausdorff derivative operator and adopted the improved salp group algorithm to determine the model parameters, and the new model was successfully used to predict the actual landslide displacement. Lizheng et al. [23] proposed a low-cost landslide displacement prediction method, which used time series measurements of acoustic emission (AE) and rainfall to predict the displacement, and they verified the effectiveness of the proposed method with a landslide that occurred in Hollin Hill, North Yorkshire, UK. Xinli et al. [24] combined empirical and data methods, and a displacement prediction method was constructed based on the Verhulst inverse function (VIF) and the random forest (RF) algorithm. The performance of the model was evaluated using RMSE and MAPE.

Since landslide displacement changes gradually over time, experts have used the time analysis method to analyze the landslide displacement in many studies [25–35]. Because the moving average (MA) method has the advantage of eliminating the accidental change factors and determining the development trend of things, it is used to analyze the landslide displacement in time and decompose the landslide displacement into trend displacement and periodic displacement for forecasting. Rubin et al. [25] built a landslide displacement prediction model by combining the ELM model with the RS-SVR model of random search support vector regression. They used the ELM model and RS-SVR model to predict the trend displacement and periodic displacement, respectively, and then they summed the two results to obtain the predicted total displacement. Yonggang et al. [26] used a cubic polynomial to predict trend displacement and the GRU model to predict periodic displacement and applied it to the Erdaohe landslide, which achieved good results. Beibei et al. [27] selected input data by calculating the grey correlation degree, and the LSTM model predicted the periodic displacement and used the real data of the Baishuihe landslide and Bazimen landslide to simulate and test the performance of the model. Fasheng et al. [28] established a dynamic model based on displacement observations and used GA-SVR to predict periodic and random terms in displacement. Although the prediction accuracy of random terms is not high, the trend can be reflected to a certain extent, which is helpful for landslide prediction. Zhongqiang et al. [29] used three prediction models, GRU, RF, and LSTM, to verify and compare the prediction effects of three landslides in the Three Gorges

area, which illustrated the effectiveness of the three models in landslide displacement prediction. Yankun et al. [30] compared five commonly used machine learning prediction models on three landslide datasets. The Hodrick–Prescott filter was used to decompose landslide displacement into trend displacement and periodic displacement, and double exponential smoothing was used to predict trend displacement. The results show that no model is optimal for the three landslides at the same time, and different models should be selected for different landslides. Zian et al. [31] improved the time series analysis method of landslides, using the WMA method to decompose the landslide displacement and the LSTM model to predict the trend displacement, and obtained good results. Subsequently, Zian et al. [32] further analyzed the composition of landslide displacement and improved the theoretical method, using the EWMA method to decompose and the Double-BiLSTM model to predict landslide displacement, which greatly improved the prediction results. Zizheng et al. [33] and Qi et al. [34] both used the variational mode decomposition (VMD) method, which is a data evaluation and decomposition method that adaptively realizes the frequency domain division of the signal and the effective separation of each component. Zizheng et al. [33] used VMD combined with a periodic neural network model, and Qi et al. [34] used the VMD method combined with the WA-GWO-BP model to achieve the accurate prediction of landslide displacement. Shiluo et al. [35] used the EMD method to decompose Baijiabao landslide displacement data, and one-step-ahead prediction and multistep-ahead prediction methods were used for prediction.

However, the method of time series analysis also has its shortcomings. In the analytical process, the existence of random displacement will be ignored because the model cannot accurately predict random displacement. To solve the shortcomings of the time series analysis method, some experts propose the time frequency analysis method, which does not ignore any part of the data and can effectively improve the accuracy of landslide displacement measurements [36–38]. Zhenglong et al. [36] and Chao et al. [37] divided landslide displacement into subsequences with different frequencies based on wavelet transform theory. Faming et al. [38] improved wavelet transform theory by using the DWT discrete wavelet transform to decompose landslide displacement, using chaos theory to reconstruct each frequency, and finally using the ELM model for prediction.

Most of the previous landslide displacement models adopted the time series method, taking landslide displacement as the data changing with time. Although those models based on the time series method can predict landslide displacement, the method has a disadvantage of ignoring random displacement. In addition, when selecting the input variables of the prediction model, only one correlation calculation method is usually used, which leads to insufficient comprehensiveness. And the choice of the displacement prediction model cannot take into account the temporal and spatial attributes of the data.

In this paper, a landslide displacement prediction model based on time–frequency analysis is proposed. This model uses the complete ensemble empirical mode decomposition with adaptive noise (CEEMDAN) method to analyze landslide displacement, which can overcome the defects of the time series method. The model adopts the joint correlation degree calculation method GRA–MIC to select the influencing factors of displacement, and considers the input variables of the model from multiple perspectives. Finally, combining the advantages of the CNN model and the BiLSTM model in data processing, the CNN–BiLSTM model is constructed to effectively extract the spatiotemporal characteristics of the data, and finally achieve accurate displacement prediction. The research results in this paper lay a foundation for the technical progress of landslide monitoring and early warning systems in the future as an important part of disaster prevention and land use management.

The main contributions of this paper are described as follows:

1. According to the principle of time frequency analysis, the CEEMDAN method [39–41] is used to decompose the landslide displacement into multiple subsequences. In this method, the original data are decomposed into different frequency data series

with local characteristics, and the data characteristics of each frequency in landslide displacement are highlighted.

2. This paper analyzes the landslide situation in the study area and proposed two new concepts, using the landslide displacement of the previous month to represent the current state of the landslide and quantifying the difference between two consecutive months of displacement data as the trend of landslide change, adding relevant data of landslide prediction and creating conditions for improving the performance of landslide prediction.
3. To consider the factors affecting landslide displacement more comprehensively, this paper combines two correlation degree calculation methods, GRA [42–44] and MIC [45,46], to obtain the GRA–MIC method. This method comprehensively selects the influencing factors from two perspectives, which is helpful to further improve the accuracy of the landslide displacement prediction model.
4. Combined with the ability of the CNN model [47] to extract local features of data and the BiLSTM model [48,49] to process time series data, the CNN–BiLSTM model was constructed to predict landslide displacement. This paper combines the two models to effectively improve the prediction performance [50].

2. Materials and Methods

2.1. Complete Ensemble Empirical Mode Decomposition with Adaptive Noise

Compared with EEMD, the CEEMDAN method adds adaptive white Gaussian noise at each stage in the decomposition process and obtains each modal component by calculating the unique margin signal. The decomposition process is complete, and the reconstruction error is extremely low [39]. The CEEMDAN method can effectively solve the mode aliasing problem of EMD and overcome the problems of low decomposition efficiency of EEMD and difficulty in completely eliminating noise [40].

$E_j(\cdot)$ is defined as the j th mode functions obtained by the EMD algorithm, $X(t)$ is the original data series, and $n^i(t)$ is the i th added white Gaussian noise satisfying the standard normal distribution. The implementation steps of the CEEMDAN method are given as follows [41]:

- (1) Similar to EEMD, the signal $X(t) + \varepsilon_0 n^i(t)$ is decomposed n times by EMD in the CEEMDAN method, and the first mode functions are obtained by mean calculation:

$$\overline{IMF_1(t)} = \frac{1}{N} \sum_{i=1}^N IMF_1^i(t) \quad (1)$$

- (2) Calculate the first margin signal $r_1(t)$ as

$$r_1(t) = X(t) - \overline{IMF_1(t)} \quad (2)$$

- (3) The EMD algorithm is used to decompose the signal $r_1(t) + \varepsilon_1 E_1(n^i(t))$ n times and then obtain the second mode functions as

$$\overline{IMF_2(t)} = \frac{1}{N} \sum_{i=1}^N E_1(r_1(t) + \varepsilon_1 E_1(n^i(t))) \quad (3)$$

- (4) For $k = 2, \dots, K$, calculate the k th residual signal as

$$r_k(t) = r_{k-1}(t) - \overline{IMF_k(t)} \quad (4)$$

- (5) The calculation process of step (3) is repeated, and the $k + 1$ mode functions are obtained as

$$\overline{IMF_{k+1}(t)} = \frac{1}{N} \sum_{i=1}^N E_1(r_k(t) + \varepsilon_k E_k(n^i(t))) \quad (5)$$

- (6) Steps (4) and (5) are repeated until the residual signal meets the termination condition of the decomposition, and K mode functions are finally obtained. The final residual signal of the decomposition is

$$R(t) = X(t) - \sum_{k=1}^K \overline{IMF_k(t)} \quad (6)$$

Then, the final original data signal can be decomposed into

$$X(t) = \sum_{k=1}^K \overline{IMF_k(t)} + R(t) \quad (7)$$

After the CEEMDAN method has been used to decompose the landslide displacement, each displacement component will be predicted separately in this paper.

2.2. Grey Relation Analysis and Maximal Information Coefficient

The basic idea of grey relation analysis theory is to judge the degree of correlation between factors according to the degree of similarity between curves, which can be used to quantitatively analyze the dynamic development process of the system to determine the degree of contribution of factors to a certain behavior or index [42]. In essence, grey correlation analysis is used to find the main relationship between various factors and determine the relevant factors that cannot be ignored to grasp the main contradiction of the development of things. Grey correlation analysis includes the following three elements: the main sequence, subsequence, and correlation degree. When the method is used to analyze the influence degree, the main sequence is generally the main behavior or index used to evaluate the system performance. The subsequence is made up of the various factors that affect the system performance. The correlation degree is the correlation degree between subsequence and main sequence obtained by grey correlation analysis [43]. In this paper, landslide displacement is selected as the main sequence, and four subsequences constitute sequence X . $X = [X_0, X_1, X_2, X_3, X_4] = [\text{landslide displacement, precipitation, reservoir level, trend of landslide, state of landslide}]$. The analysis and selection of the factors influencing landslide displacement are presented in Section 3.2 of this paper. The process of GRA is described as follows [44].

Because the physical interpretation of each type of data is different, resulting in different ranges of resulting data, it is not suitable for direct comparison. Therefore, data normalization needs to be performed in GRA. The following equation is the normalization method for the data:

$$X_i(k)' = X_i(k) / \frac{1}{n} \sum_{i=1}^N X_i(k) \quad (8)$$

where $i = 0, 1, \dots, m; k = 0, 1, \dots, n$, M is the number of types of influencing factors, and N is the number of data affecting factors. After data normalization, correlation coefficients between landslide displacement and the other four influencing factors and grey relational grade could be calculated as follows:

$$\xi(x_0(k)', x_i(k)') = \frac{\min_i \min_k |x_i(k)' - x_0(k)'| + \rho \min_i \min_k |x_i(k)' - x_0(k)'|}{|x_i(k)' - x_0(k)'| + \rho \max_i \max_k |x_i(k)' - x_0(k)'|} \quad (9)$$

$$r(x_0, x_i) = \frac{1}{n} \sum_{k=1}^n \xi(x_0(k)', x_i(k)') \quad (10)$$

where $\xi(x_0(k)', x_i(k)')$ is the correlation coefficient between x_i and the sequence x_j , ρ is the resolution coefficient, the usual value is 0.5, and $r(x_0, x_i)$ is the final grey relational grade. Generally, factors with GRD > 0.65 are considered to be important influencing factors [51].

The maximal information coefficient (MIC) was proposed by Reshef et al. [45] in 2011, and it is developed based on mutual information (MI). Mutual information can be regarded as the uncertainty of a random variable reduced by the knowledge of another random variable, which is mainly used to measure the degree of correlation between linear or nonlinear variables, and its value range is [0, 1]. If x and y are random variables, the mutual information is defined as

$$I(x; y) = \sum_x \sum_y p(x, y) \log \frac{p(x, y)}{p(x)p(y)} \quad (11)$$

where $I(x; y)$ is the mutual information of variables x and y , $p(x, y)$ is the joint probability density function, and $p(x)$ and $p(y)$ are the marginal density functions. The greater the mutual information between the two variables is, the stronger the correlation is [46]. Compared with mutual information, MIC overcomes the disadvantage that mutual information cannot be used to conveniently calculate continuous variables based on MI, and it has a higher accuracy. MIC is a normalized maximum mutual information with low computational complexity, good robustness, and higher accuracy than mutual information. When sufficient statistical samples are available, MIC can capture a wide range of relationships and better reflect the degree of association between attributes and features [52]. The scatterplot composed of random variables x and y in two-dimensional space is gridded in m columns and n rows, and then the MIC formula is:

$$MIC(x; y) = \max_{m*n < B(n)} \left(\sum_x \sum_y p(x, y) \log \frac{p(x, y)}{p(x)p(y)} / \log \min(m, n) \right) \quad (12)$$

where $m * n < B(n)$ represents the constraints on the total number of meshes, and $B(n)$ is usually set to $n^{0.6}$. The greater the MIC value between the two variables is, the stronger the correlation is. Conversely, for the opposite, the weaker the correlation is. Generally, factors with $MIC > 0.3$ are considered to be important influencing factors [48].

To better select the factors influencing landslide displacement, the factors selected in this study need to meet both $GRG > 0.65$ and $MIC > 0.3$.

2.3. CNN–BiLSTM Model

A convolutional neural network (CNN) is a feedforward neural network [53]. A typical CNN model is shown in Figure 1. It includes an input layer, convolutional layer, pooling layer, fully connected layer, and output layer.

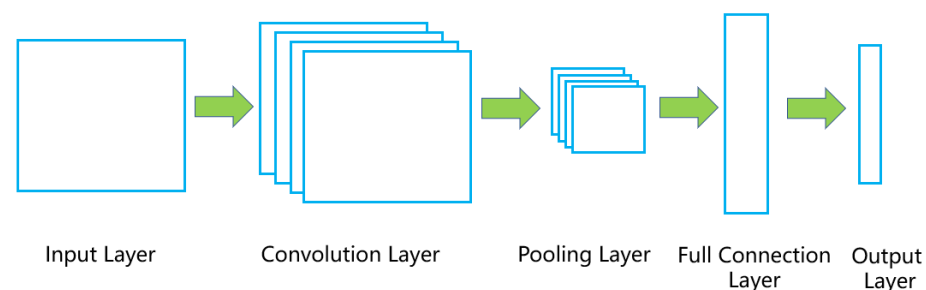


Figure 1. Structure of the CNN model.

The essence of the CNN model lies in the construction of multiple filters that can extract data features, and the hidden topological features among data can be extracted through layer-by-layer convolution and pooling of input data [47]. As the number of layers increases, the extracted features become increasingly abstract. Finally, these abstract features are merged through fully connected layers, and the classification and regression problems are solved by softmax or sigmoid activation functions. One of the characteristics of the CNN model is that it can extract local features of input data [54]. Moreover, the

high-level features are abstracted and combined layer by layer, which can effectively realize feature extraction in a complex landslide environment.

The LSTM model is a variant of the RNN model that transmits forward information and processes current information. The LSTM model introduces a new internal state to transmit linear cyclic information, outputs information to the hidden state, and selects to retain or forget information through three control gate units (input gate, forget gate, and output gate) [55]. The input gate controls how much input information needs to be retained at the current time. The forget gate controls how much information needs to be discarded at the last moment. The output gate controls how much information needs to be output to the hidden state at the current time [56]. Although the LSTM model can obtain the feature information over a long distance, the information it obtains is the information obtained before the output time, instead of using the reverse information, while the BiLSTM model can use the past and future information to make more perfect and detailed decisions [49]. The BiLSTM model is an improved version of the LSTM model, which is very suitable for processing time series data [48]. The BiLSTM model is formulated as follows:

$$f_t = \sigma(W_f x_t + U_f h_{t-1} + b_f) \quad (13)$$

$$\tilde{c}_t = \tanh(W_c x_t + U_c h_{t-1} + b_c) \quad (14)$$

$$i_t = \sigma(W_i x_t + U_i h_{t-1} + b_i) \quad (15)$$

$$c_t = f_t \odot c_{t-1} + i_t \odot \tilde{c}_t \quad (16)$$

$$o_t = \sigma(W_o x_t + U_o h_{t-1} + b_o) \quad (17)$$

$$\vec{h}_t = \text{LSTM}(h_{t-1}, x_t, c_{t-1}), t \in [1, T] \quad (18)$$

$$\overleftarrow{h}_t = \text{LSTM}(h_{t+1}, x_t, c_{t+1}), t \in [T, 1] \quad (19)$$

$$H_t = \begin{bmatrix} \vec{h}_t & \overleftarrow{h}_t \end{bmatrix} \quad (20)$$

where x_t , f_t , i_t , o_t , h_t , C_t , and \tilde{C}_t denote the input data, forget gate, input gate, output gate, output data, cell state, and temporary state of the cell, respectively; w_f , w_o , w_i , and w_c denote the weight of the forget gate, the weight of the output gate, the weight of the input gate, and the weight of the temporary state, respectively; and b_f , b_i , b_o , and b_c represent the bias of the forget gate, the bias of the input gate, the bias of the output gate, and the bias of the temporary state, respectively. $[\]$ is the connection between two vectors, \tanh is the tanh function, σ is the sigmoid function, \odot is the matrix product, and \vec{h}_t and \overleftarrow{h}_t are the outputs of BiLSTM in two directions. H_t is the output of BiLSTM. Figure 2 shows the BiLSTM architecture.

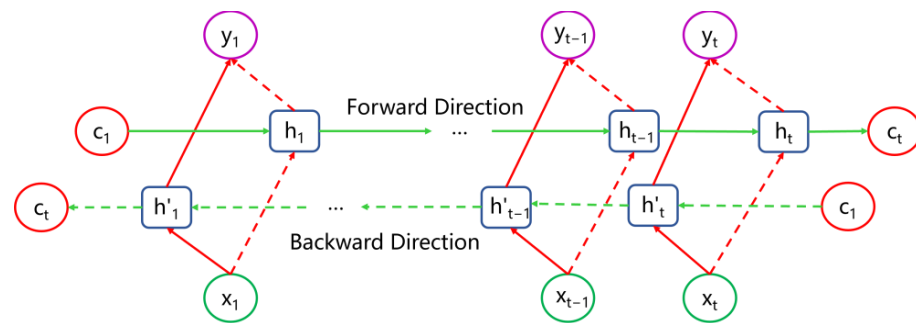


Figure 2. Structure of the BiLSTM model.

CNN and BiLSTM are both mainstream deep learning models. CNN is more suitable for spatial expansion, extracting local data features, and combining and abstracting them into high-level features. BiLSTM is more suitable for time expansion; it has long-term memory function, and it is more suitable for processing time series. In the feature extraction of landslide displacement and environmental factor data, it is necessary to consider not only the spatial relationship between different parameters, but also the change in data in the temporal dimension. Therefore, this paper combines the CNN and BiLSTM models to propose a CNN–BiLSTM model, which enables the model to express features spatiotemporally. The structure of the proposed model is shown in Figure 3.

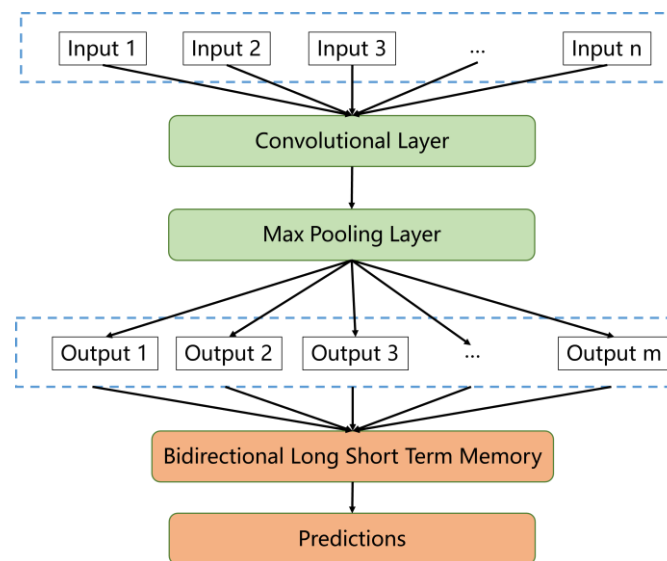


Figure 3. Structure of the CNN–BiLSTM model.

2.4. Performance Indicators

To evaluate the prediction effect of different artificial intelligence models, a variety of indicators can be used to verify model performance [57]. In this paper, the root mean square error (RMSE), mean absolute error (MAE), mean absolute percentage error (MAPE), and correlation coefficient R^2 were used to reflect the prediction effect.

$$MSE = \sqrt{\frac{1}{n} \sum_{i=1}^n (\hat{y}_i - y_i)^2} \quad (21)$$

$$MAE = \frac{1}{n} \sum_{i=1}^n |\hat{y}_i - y_i| \quad (22)$$

$$MAPE = \frac{100\%}{n} \sum_{i=1}^n \left| \frac{\hat{y}_i - y_i}{y_i} \right| \quad (23)$$

$$R^2 = 1 - \frac{\sum_{i=1}^n (\hat{y}_i - y_i)^2}{\sum_{i=1}^n (\bar{y}_i - y_i)^2} \quad (24)$$

where $\hat{y} = \{\hat{y}_1, \hat{y}_2, \dots, \hat{y}_n\}$ is the predicted value, $y = \{y_1, y_2, \dots, y_n\}$ is the measured value, $\bar{y} = \{\bar{y}_1, \bar{y}_2, \dots, \bar{y}_n\}$ is the average of the measurements, and n is the number of samples. The model is judged according to the results of *RMSE*, *MAE*, *MAPE* and R^2 , and the value range of the results is $[0, 1]$. The closer to 0 the values of the first three evaluation indexes are, the better the prediction performance of the model is. The closer to 1 R^2 is, the better the prediction performance of the model is.

3. Results

3.1. Real Case

The Baishuihe landslide is located on the right bank of the Yangtze River in Zigui County, Three Gorges Reservoir Area, 56 km away from the Three Gorges Dam, $110^{\circ}32'09''$ east longitude, $31^{\circ}01'34''$ north latitude [58]. Surrounded by mountains on three sides and water on one side, it is very conducive to the collection of rainfall. The elevation of the terrain gradually increases from north to south, with a difference of approximately 330 m. The landslide is approximately 700 m wide from east to west and divided by bedrock ridges on both sides. It runs north–south and has a length of approximately 770 m. The overall slope of the landslide ranges from 30° to 35° , the average thickness is 30 m, and the volume is approximately $1260 \times 104 \text{ m}^3$. The Baishuihe landslide is an accumulation-type, soil-like landslide with a loose structure; the sliding body is mainly composed of gravel soil and silty clay mixed with gravel, the sliding zone soil is mostly silty clay mixed with gravel or breccias, the underlying bedrock is argillaceous siltstone, mostly in the form of moderate weathering, and the joint and fracture development is relatively obvious. The terrain is stepped, steeper in the upper part and gentle in the middle, creating favorable conditions for the accumulation of colluvial materials. The Baishuihe landslide is a flat transition slide, and the thickness of the sliding body gradually increases from the rear edge to the forward edge, especially in the middle and front of the landslide. Due to the small deformation of the rear part of the landslide, it is in a relatively stable stage, so the main risk of landslide is concentrated in the warning area of the landslide front. There are obvious macroscopic deformations and house cracking on the surface of the landslide in Baishuihe, and the nearby villagers have been relocated. Now, the risk of Baishuihe landslide is mainly a threat to passing boats and roads within the landslide. Eleven Global Positioning System (GPS) monitoring points were installed on the Baishuihe landslide. Since the ZG118 monitoring point was installed in the central area of the whole Baishuihe landslide, it can better reflect the situation of the Baishuihe landslide. Therefore, other studies also use data from the ZG118 monitoring point [59]. The data of two horizontal directions and one vertical direction are monitored for Baishuihe landslide monitoring points, and the final displacement value is a vector calculation value of three directions. Rainfall is based on the data from a local weather station. The reservoir water level is based on the data provided by the Three Gorges hydrology station. The distribution of GPS monitoring points is shown in Figure 4.

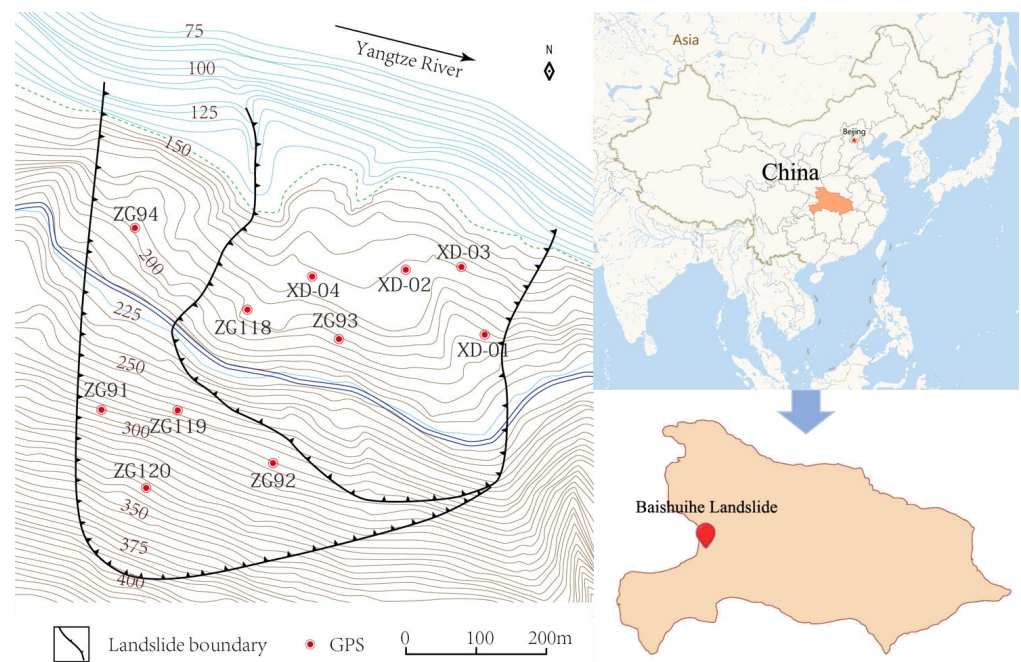


Figure 4. GPS installation positions.

In this paper, the rainfall data and reservoir water level data of the Baishuihe landslide in the same period were monitored and recorded once a month. The time range was from January 2004 to December 2012, with a total of 108 data points, as shown in Figure 5.

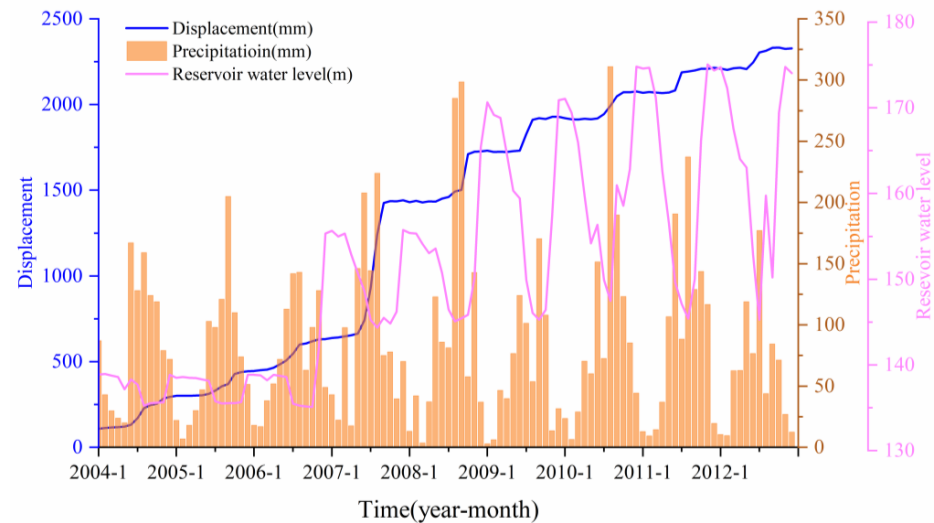


Figure 5. Displacement and environmental data variation in the Baishuihe landslide.

In this paper, the first 96 data points were used as the training data for the model, and the last 12 data points were used as the prediction data for the model test set. The prediction results were compared with the actual measured data to evaluate the prediction performance of the model.

3.2. Analysis of Factors Influencing Landslide Displacement

The Three Gorges area, where the Baishuihe landslide is located, is part of the subtropical monsoon climate zone, with precipitation concentrated from April to August and typically very little rainfall from January to March. Based on the historical data, when rainfall increases, landslide displacement also increases, and when rainfall is scarce, landslide displacement hardly changes. The reason is that a large amount of rain washes the

landslide and drives the soil on the slope to slide downward. The rain enters the landslide, increasing the weight of the landslide and increasing the possibility of land sliding. A large amount of rainwater infiltration leads to the saturation of the soil and rock layer on the slope, and even water accumulation on the waterproof layer at the lower part of the slope, thus increasing the weight of the sliding body and reducing the shear strength of the soil and rock layer, resulting in landslides. When studying landslides, many researchers consider rainfall to be one of the influencing factors [16,60], and some scholars also consider rainfall to be the most important influencing factor [61].

Figure 5 shows that the landslide displacement changed the most in 2007, but the rainfall was the largest in 2008 and 2010, which indicates that in addition to rainfall there are other factors that also affect landslide displacement. Because the Baishuihe landslide is on the right bank of the Yangtze River, close to the Three Gorges Dam, it is easily affected by the release of water from the dam. Whenever the Three Gorges Dam opens the sluice to release water, the water level of the reservoir drops and the water level of the Yangtze River rises rapidly, impacting the surface of the Baishuihe landslide, and water flows into the slope, increases the pore water pressure, softens the rock and soil, and increases the bulk density of the landslide. The overall structure of the landslide has an impact that promotes or induces the occurrence of land sliding.

The geological conditions of landslides are complex, and there is no clear and unified standard. According to previous studies, landslides exist in a variety of different states, and the corresponding stability of different states is also different [14,29]. The cumulative displacement–time curve of the Baishuihe landslide presents an obvious ladder-like pattern. In particular, the height of the ladder was highest in 2007. The maximum displacement velocity of the Baishuihe landslide is greater than 26 mm/day, and the average annual deformation rate is also above 250 mm. The displacement of the landslide moved slowly from 2004 to 2006, and the displacement accelerated obviously in 2007. However, the deformation speed dropped again at the beginning of 2008, and the displacement grew slowly. The fastest increase in the deformation rate of the landslide occurred in July 2007, which coincided with the decrease in rainfall and reservoir water level during this period. We believe that the magnitude of landslide displacement is related to the stability of the landslide. When the landslide is in a stable state, it is difficult for external factors to lead to the occurrence of landslide displacement. When the landslide is in an unstable state, relatively minor factors may lead to a more serious landslide collapse phenomenon. Therefore, the landslide displacement can reflect a certain landslide state. This paper intends to use the displacement of the previous month to represent the current state of the landslide and participate in the prediction of landslide displacement.

Due to the influence of the landslide itself and environmental factors, it usually produces a certain displacement every month. If the displacement of the previous month is taken as the current state of the landslide, the difference in the displacement data of two consecutive months is considered to be the change between the two states of the landslide, which reflects the development trend of the landslide to a certain extent. When the change is large, it reflects the development direction of the landslide, indicating that the landslide is in a trend of unstable development and can change violently. To improve the accuracy of landslide displacement prediction, this paper attempts to quantify the difference between two consecutive months of displacement data as the trend of landslide change, which is considered to be one of the inputs of the prediction model.

The selection of influencing factors will directly affect the training and prediction ability of the model [28]. Based on the above analysis, this study believes that the development of landslide displacement is the result of the influence of rainfall, reservoir water level, landslide trend and landslide state. Therefore, this paper considers these four factors to be the factors influencing landslide displacement.

3.3. Decomposition of Original Data

For the raw data, the CEEMDAN method decomposition training set of landslide displacement, rainfall, and reservoir water level, with the status and trend of landslide data, namely, 96 consecutive data points for decomposition, was used. The decomposition of landslide displacement will obtain three components, the decomposition of rainfall will obtain five components, the decomposition of the reservoir water level will obtain four components, the decomposition of landslides will obtain three state variables, and the decomposition of the landslide trend will yield six components. The results breakdown is shown in Figures 6–11.

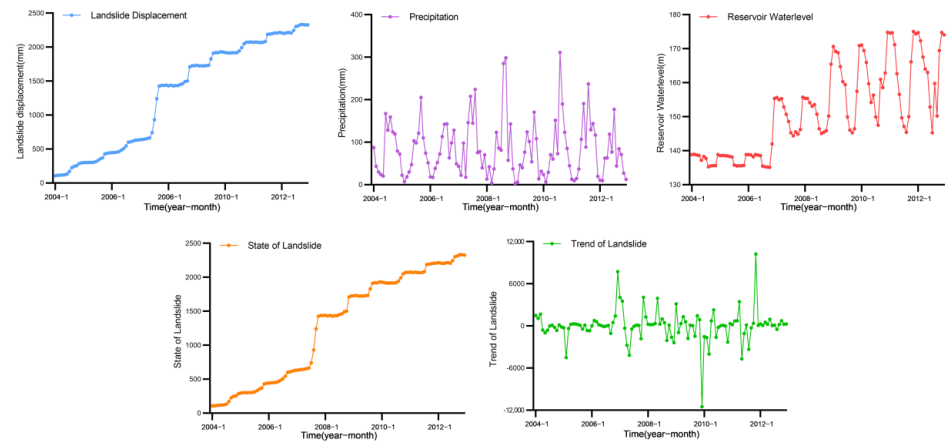


Figure 6. Original data of Baishuihe landslide.

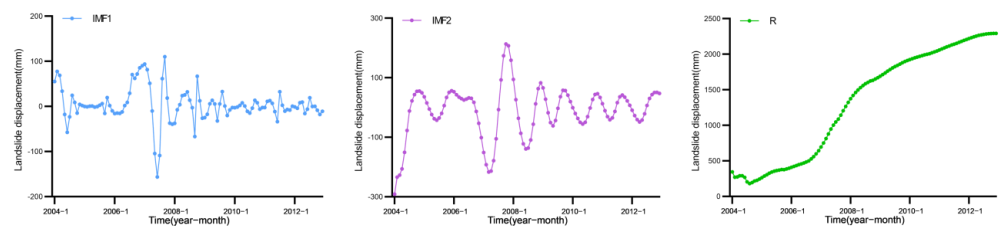


Figure 7. CEEMDAN method decomposing original landslide displacement data results.

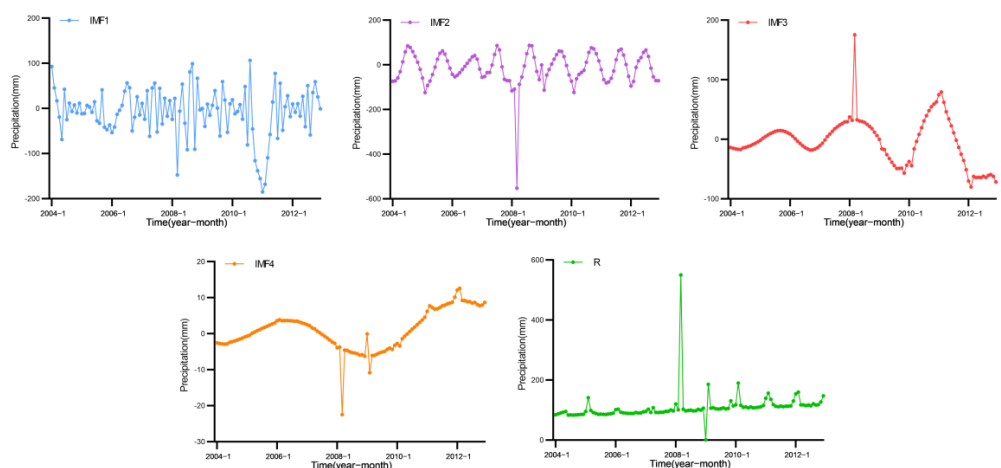


Figure 8. CEEMDAN method decomposing original precipitation data results.

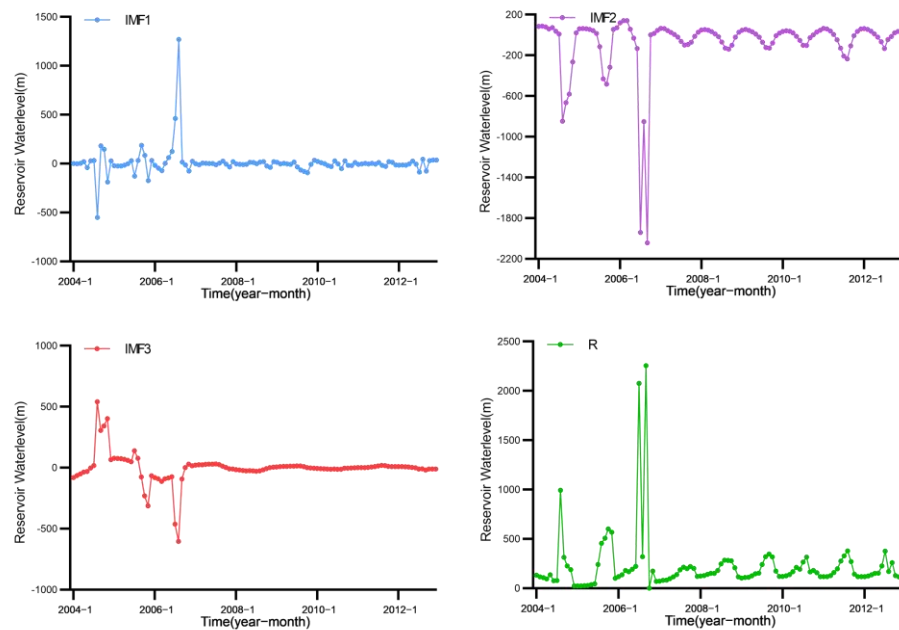


Figure 9. CEEMDAN method decomposing reservoir water level original data results.

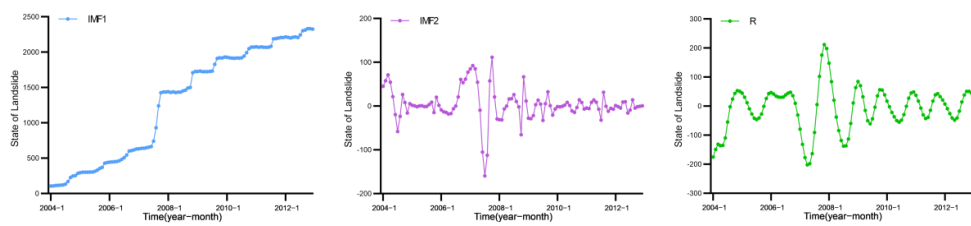


Figure 10. CEEMDAN method decomposing original state data results.

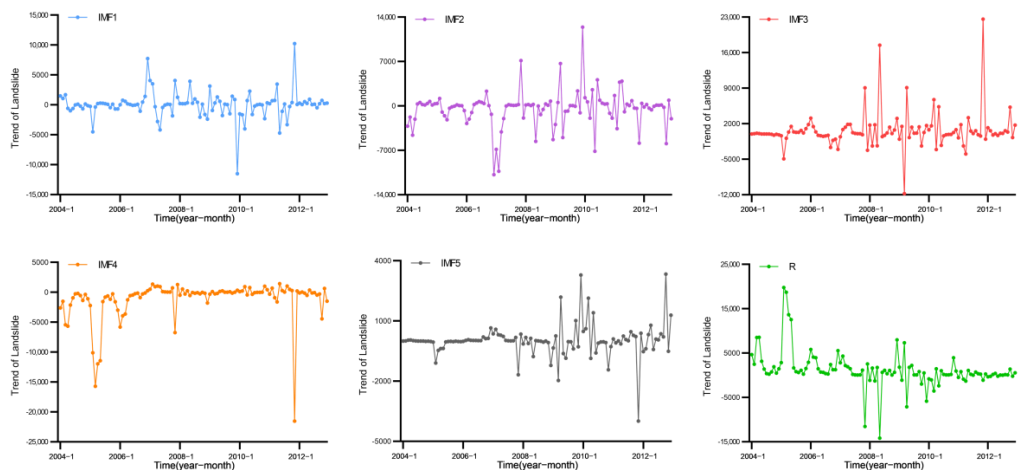


Figure 11. CEEMDAN method decomposing original trend data results.

3.4. GRA–MIC Algorithm Calculation of the Correlation

After the landslide displacement had been decomposed by the CEEMDAN method, multiple subsequences with different frequencies could be obtained. However, not all factors had an effect on landslide displacement. Using factors with less influence on landslide displacement to train the prediction on model will reduce the prediction accuracy, while using factors with greater influence will help improve the prediction performance of the model. Many studies use the MIC algorithm or GRA algorithm to calculate the

correlation degree between landslide displacement and environmental factors [61,62], and both algorithms quantify the correlation degree from their own single perspective. Considering these two algorithms, this study proposes a GRA–MIC algorithm and, when combined with the GRA algorithm and the MIC algorithm, it can consider the correlation between displacement and environmental factors from two perspectives and improve the prediction accuracy. Moreover, in the Discussion section, the prediction is compared with that using the GRA algorithm or the MIC algorithm alone. The correlation calculation results are shown in Tables 1 and 2.

Table 1. GRA between landslide displacement and influencing factors.

Landslide Displacement	Influencing Factors	Influencing Factor Subsequences					
		IMF1	IMF2	IMF3	IMF4	IMF5	IMF6
IMF1	Precipitation	0.794	0.712	0.715	0.674	0.622	/
	Reservoir water level	0.791	0.782	0.712	0.623	/	/
	State of landslide	0.904	0.805	0.625	/	/	/
	Trend of landslide	0.887	0.836	0.735	0.721	0.749	0.671
IMF2	Precipitation	0.755	0.691	0.707	0.672	0.616	/
	Reservoir water level	0.755	0.738	0.689	0.622	/	/
	State of landslide	0.793	0.904	0.623	/	/	/
	Trend of landslide	0.804	0.797	0.724	0.701	0.703	0.627
R	Precipitation	0.620	0.619	0.590	0.623	0.900	/
	Reservoir water level	0.638	0.639	0.616	0.927	/	/
	State of landslide	0.605	0.603	0.989	/	/	/
	Trend of landslide	0.623	0.628	0.602	0.726	0.607	0.491

Table 2. MIC between landslide displacement and influencing factors.

Landslide Displacement	Influencing Factors	Influencing Factor Subsequences					
		IMF1	IMF2	IMF3	IMF4	IMF5	IMF6
IMF1	Precipitation	0.194	0.212	0.264	0.269	0.337	/
	Reservoir water level	0.263	0.235	0.290	0.337	/	/
	State of landslide	0.338	0.266	0.337	/	/	/
	Trend of landslide	0.304	0.291	0.247	0.273	0.329	0.337
IMF2	Precipitation	0.255	0.300	0.337	0.482	0.531	/
	Reservoir water level	0.268	0.238	0.331	0.381	/	/
	State of landslide	0.319	0.757	0.531	/	/	/
	Trend of landslide	0.179	0.304	0.306	0.303	0.400	0.512
R	Precipitation	0.309	0.370	0.954	0.852	0.913	/
	Reservoir water level	0.423	0.468	0.837	0.789	/	/
	State of landslide	0.323	0.538	0.679	/	/	/
	Trend of landslide	0.236	0.382	0.598	0.978	0.842	0.877

After obtaining the results of the correlation calculation with the GRA–MIC algorithm, it is necessary to select appropriate factors to participate in the training and prediction of the model. Selecting factors with a correlation that is too low will result in the selection of too many data that are not related to landslide displacement, which will reduce the accuracy of the landslide displacement prediction. Although the selection of factors with a high correlation is beneficial to the prediction process, there are few qualified data, which will lead to insufficient training of the model, affecting the prediction performance of the model. In this paper, data satisfying the conditional $GRA > 0.65$ and the conditional $MIC > 0.3$ were selected.

3.5. Predicted Landslide Displacement

According to the results in Tables 1 and 2, the input data of the IMF1 component of landslide prediction finally selected six influencing factor subseries, the input data of the IMF2 component of landslide prediction finally selected nine influencing factor subseries, and the input data of the R component of landslide prediction finally selected

five influencing factor subseries. The first 96 selected data were used to train the CNN–BiLSTM model, and the last 12 data were used to test the prediction accuracy. The learning rate of the CNN–BiLSTM model was set to 0.01, the number of iterations was set to 1000, and the number of hidden stratification points was set to 100. The prediction results of the three components of landslide displacement are shown in Figure 12a–c. The final predicted landslide displacement can be obtained by adding the three components, as shown in Figure 12d. The prediction model proposed in this paper can predict the displacement of the Baishuihe landslide.

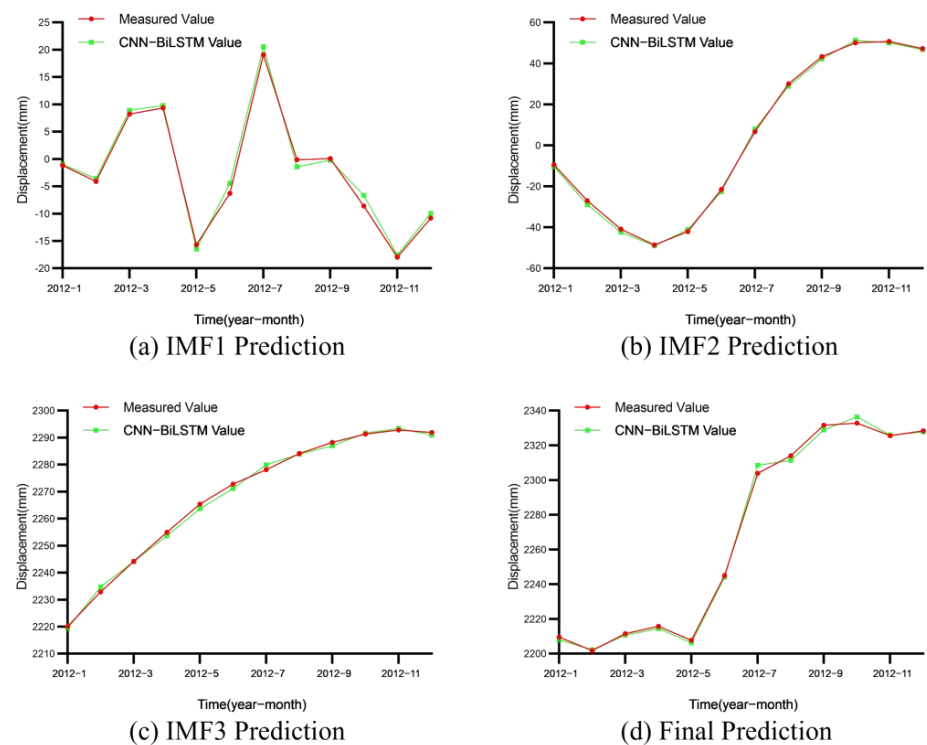


Figure 12. Prediction result of the CNN–BiLSTM model for the Baishuihe landslide displacement.

After the GRA–MIC algorithm screening, the CNN–BiLSTM model could achieve good results in both the displacement component and total displacement prediction, and the error between the final results and the actual measured data was controlled within a limited range.

4. Discussion

To better verify the performance of the proposed model, when other conditions are the same, in this paper, CNN–BiLSTM with GRA–MIC, CNN–BiLSTM with MIC, CNN–BiLSTM with GRA and CNN–BiLSTM without GRA–MIC were used to predict and compare the three components of landslide displacement. The comparison results of the CNN–BiLSTM model for each component and the total displacement are shown in Figure 13.

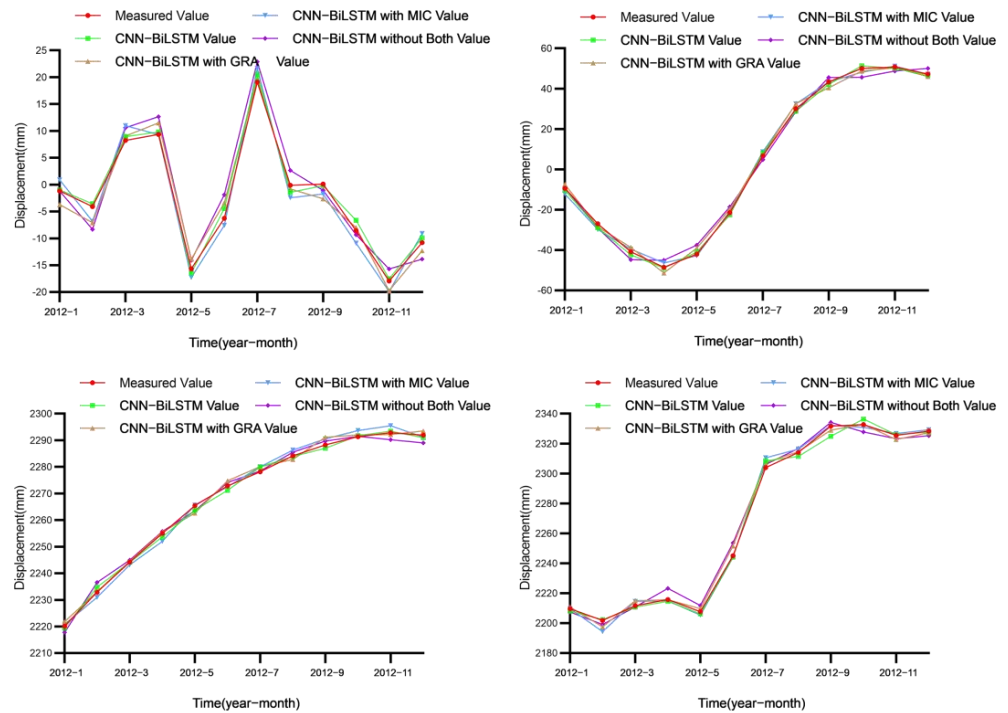


Figure 13. Prediction results of CNN–BiLSTM model with different inputs.

When the CNN–BiLSTM model was used for prediction, good prediction results could be achieved under different quantitative correlation algorithms, which reflects the excellent prediction performance of the CNN–BiLSTM model. For a better comparison, this paper uses four evaluation indicators to quantify the prediction performance, and the comparison results are shown in Table 3.

Table 3. Comparison of prediction performances of the CNN–BiLSTM model under different inputs.

Models	MAE	MAPE	RMSE	R ² (%)	Minimum Error	Maximum Error	Total Error
CNN–BiLSTM	1.789	0.078	2.206	99.84	0.02	6.77	25.62
CNN–BiLSTM with GRA	2.335	0.103	2.981	99.70	0.02	6.54	28.02
CNN–BiLSTM with MIC	2.323	0.102	3.240	99.65	0.18	7.51	28.04
CNN–BiLSTM without Both	3.630	0.161	4.238	99.40	0.82	8.52	43.56

As shown in Table 3, when the GRA or MIC algorithms were used, appropriate influencing factors could be effectively selected, and the result was better than that when neither of the two algorithms were used, which reflects the role played by the GRA and MIC algorithms. When the GRA–MIC algorithm was used in the model, better influencing factors were selected from two different perspectives, and data with low correlations were removed. Compared with the GRA or MIC algorithms, the prediction results of the model were further improved. Due to the reduction in input data, the GRA–MIC algorithm not only improved the efficiency of the whole prediction process of the model, but also improved the prediction performance of the model.

In addition to comparing the prediction performance of the CNN–BiLSTM model in different correlation algorithms, this paper also used an additional seven deep learning algorithms for comparison: the CNN–RNN, CNN–LSTM, CNN–GRU, BiLSTM, RNN, LSTM, and GRU models. In the case of the GRA–MIC algorithm and other identical cases, the results comparisons of the eight models are shown in Figure 14 and Table 4.

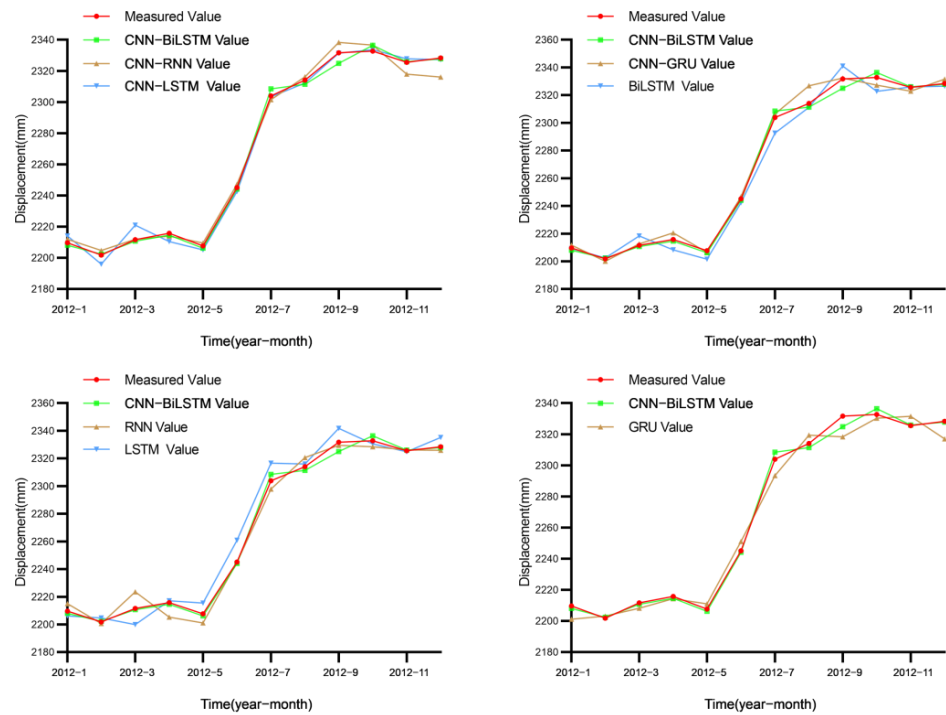


Figure 14. Comparison of the prediction effect between the CNN–BiLSTM model and other models.

Table 4. Comparison of prediction performances of different models with the same input.

Models	MAE	MAPE	RMSE	R ² (%)	Minimum Error	Maximum Error	Total Error
CNN–BiLSTM	1.789	0.078	2.206	99.84	0.02	6.77	25.62
CNN–RNN	3.841	0.167	5.018	99.17	0.31	12.28	46.09
CNN–LSTM	3.063	0.137	4.012	99.47	0.23	9.36	36.76
CNN–GRU	3.302	0.144	4.578	99.31	0.64	12.69	39.62
BiLSTM	5.018	0.220	6.300	98.70	0.36	11.24	60.19
RNN	5.442	0.239	7.274	98.26	0.07	11.93	58.11
LSTM	4.888	0.215	7.013	98.38	0.74	15.79	77.49
GRU	6.076	0.266	7.203	98.29	1.21	13.37	72.91

Table 4 shows that because of the complexity and uncertainty of the landslide, a suitable time series data classification of the CNN model was adopted to forecast the displacement characteristics of the future and then build other models to forecast the concrete values; the effective reduction of the single model for complex data fitting ability was insufficient, and increasing the CNN part model could obtain a better effect. Compared with RNN models, traditional LSTM and GRU models have better prediction performances because the internal gate structures of the LSTM and GRU models adjust the input data flow and solve the problems of gradient disappearance and gradient explosion. Because of the similar structures, the prediction performances of the LSTM and GRU models are similar. Since the BiLSTM model adopts a bidirectional LSTM module, it can more fully train data and extract periodic information from environmental data in the training process. Compared with the traditional LSTM model, it improves the efficiency of data use and the accuracy of prediction.

5. Conclusions

The effective analysis and utilization of landslide displacement and influencing factor data is particularly important to improve the accuracy of landslide displacement prediction and ensure early warnings of landslides. Additionally, it provides a geological theoretical basis for the policymaking of land use management. Due to the problem of random displacement being ignored in time series analysis, the accuracy of the time series analysis method is limited when it is used in rainfall landslide displacement prediction. In this paper, a rainfall landslide displacement prediction method based on the time-frequency analysis method was proposed. The CEEMDAN method was used to decompose landslide displacement data into multiple subseries with different frequencies, two new concepts that evaluate the state of the landslide and the trend of the landslide were proposed, and the GRA–MIC joint association method was used to select the main influencing factors of each subseries. Then, CNN–BiLSTM, a fusion model based on deep learning, was used to train and predict landslide displacement. The model combines the CNN model with the BiLSTM model so that the model can more fully extract the features of landslide displacement data to provide a more effective method to use landslide displacement data. The prediction of landslide displacement showed that the fusion model combining CNN and BiLSTM was more effective than the single model in predicting the landslide displacement of Baishuihe, and the GRA–MIC joint association method was better than the single method in selecting influencing factors. This paper provides a research basis for landslide early warning based on landslide displacement.

Author Contributions: Conceptualization, Z.L., Y.J. and X.S.; methodology, Z.L., Y.J. and X.S.; formal analysis, Z.L.; software, Z.L.; validation, Z.L., Y.J. and X.S.; resources, Y.J. and X.S.; writing—original draft preparation, Z.L. and X.S.; writing—review and editing, Z.L., Y.J. and X.S.; funding acquisition, Y.J. and X.S. All authors have read and agreed to the published version of the manuscript.

Funding: This research was funded by the National Natural Science Foundation of China (62161007, 62061010), Department of Science and Technology of Guangxi Zhuang Autonomous Region (AA20302022, AA19254029, AB21196041, AB22035074, AD22080061), Guilin Science and Technology Project (20210222-1).

Institutional Review Board Statement: Not applicable.

Informed Consent Statement: Not applicable.

Data Availability Statement: The datasets analyzed in the current study are available from the corresponding author on reasonable request.

Conflicts of Interest: The authors declare no conflict of interest.

References

1. Mohanty, U.C.; Prasad, K.B.; Mohapatra, M.; Sarat, C.S. Guest editorial to the special issue of natural hazards: Climate change and coastal vulnerability. *Nat. Hazards* **2020**, *102*, 553–555. [\[CrossRef\]](#)
2. Mahdi, P.; Amiya, G.; Hamid, R.P.; Fatemeh, R.; Saro, L. Spatial prediction of landslide susceptibility using hybrid support vector regression (SVR) and the adaptive neuro-fuzzy inference system (ANFIS) with various metaheuristic algorithms. *Sci. Total Environ.* **2020**, *741*, 139937.
3. Suk, W.K.; Kun, W.C.; Minseok, K.; Filippo, C.; Byoungkoo, C.; Jung, I.S. Effect of antecedent rainfall conditions and their variations on shallow landslide-triggering rainfall thresholds in South Korea. *Landslide* **2021**, *18*, 569–582.
4. Minu, T.A.; Neelima, S.; Maria, A.B.; Biswajeet, P.; Binh, T.P.; Samuele, S. Using Field-Based Monitoring to Enhance the Performance of Rainfall Thresholds for Landslide Warning. *Water* **2020**, *12*, 3453.
5. Rahat, K.; Suhail, Y.; Abdul, H.; Uddin, M.I. Exploring a Design of Landslide Monitoring System. *Complexity* **2021**, *2021*, 5552417.
6. Leijin, L.; Feng, H.; Hongjiang, L. The use of remote sensing satellite using deep learning in emergency monitoring of high-level landslides disaster in Jinsha River. *J. Supercomput.* **2021**, *77*, 8728–8744.
7. Rodriguez-Caballero, E.; Rodriguez-Lozano, B.; Segura-Tejada, R.; Blanco-Sacristán, J.; Cantón, Y. Landslides on dry badlands: UAV images to identify the drivers controlling their unexpected occurrence on vegetated hillslopes. *J. Arid. Environ.* **2021**, *187*, 104434. [\[CrossRef\]](#)
8. Moritz, G.; John, S.; Kurosch, T. Internet of Things Geosensor Network for Cost-Effective Landslide Early Warning Systems. *Sensors* **2021**, *21*, 2609.

9. Pietro, M.; Mariano, D.N.; Luigi, G.; Massimo, R.; Chester, S.; Mariagiulia, A.C.; Diego, D.M. Landslide Awareness System (LAWs) to Increase the Resilience and Safety of Transport Infrastructure: The Case Study of Pan-American Highway (Cuenca–Ecuador). *Remote Sens.* **2021**, *13*, 1564.
10. Ascanio, R.; Samuele, S.; Vanessa, C.; Antonio, M.; Angela, G.; Nicola, C. Definition of 3D rainfall thresholds to increase operative landslide early warning system performances. *Landslide* **2020**, *18*, 1045–1057.
11. National Bureau of Statistics of the People’s Republic of China. In *China Statistical Yearbook*; China Statistics Press: Beijing, China, 2021.
12. Won, Y.L.; Seon, K.P.; Hyo, H.S. The optimal rainfall thresholds and probabilistic rainfall conditions for a landslide early warning system for Chuncheon, Republic of Korea. *Landslide* **2021**, *18*, 1721–1739.
13. Wang, C.; Zhao, Y.; Bai, L.; Guo, W.; Meng, Q. Landslide Displacement Prediction Method Based on GA-Elman Model. *Appl. Sci.* **2021**, *11*, 11030. [[CrossRef](#)]
14. Liu, Y.; Xu, C.; Huang, B.; Ren, X.; Liu, C.; Hu, B.; Chen, Z. Landslide displacement prediction based on multi-source data fusion and sensitivity states. *Eng. Geol.* **2020**, *271*, 105608. [[CrossRef](#)]
15. Li, S.H.; Wu, L.; Chen, J.J.; Huang, R. Multiple data-driven approach for predicting landslide deformation. *Landslide* **2020**, *17*, 709–718. [[CrossRef](#)]
16. Wu, L.Z.; Li, S.H.; Huang, R.Q.; Xu, Q. A new grey prediction model and its application to predicting landslide displacement. *Appl. Soft Comput.* **2020**, *95*, 106543. [[CrossRef](#)]
17. Jiang, Y.; Luo, H.; Xu, Q.; Lu, Z.; Liao, L.; Li, H.; Hao, L. A Graph Convolutional Incorporating GRU Network for Landslide Displacement Forecasting Based on Spatiotemporal Analysis of GNSS Observations. *Remote Sens.* **2022**, *14*, 1016. [[CrossRef](#)]
18. Lian, C.; Zhu, L.; Zeng, Z.; Su, Y.; Yao, W.; Tang, H. Constructing prediction intervals for landslide displacement using bootstrapping random vector functional link networks selective ensemble with neural networks switched. *Neurocomputing* **2018**, *291*, 1–10. [[CrossRef](#)]
19. Long, J.; Li, C.; Liu, Y.; Feng, P.; Zuo, Q. A multi-feature fusion transfer learning method for displacement prediction of rainfall reservoir-induced landslide with step-like deformation characteristics. *Eng. Geol.* **2022**, *297*, 106494. [[CrossRef](#)]
20. Xie, P.; Zhou, A.; Chai, B. The Application of Long Short-Term Memory(LSTM) Method on Displacement Prediction of Multifactor-Induced Landslides. *IEEE Access.* **2019**, *7*, 54305–54311. [[CrossRef](#)]
21. Han, H.; Shi, B.; Zhang, L. Prediction of landslide sharp increase displacement by SVM with considering hysteresis of groundwater change. *Eng. Geol.* **2021**, *280*, 105876. [[CrossRef](#)]
22. Li, S.; Wu, N. A new grey prediction model and its application in landslide displacement prediction. *Chaos Solitons Fractals* **2021**, *147*, 110969. [[CrossRef](#)]
23. Deng, L.; Smith, A.; Dixon, N.; Yuan, H. Machine learning prediction of landslide deformation behaviour using acoustic emission and rainfall measurements. *Eng. Geol.* **2021**, *293*, 106315. [[CrossRef](#)]
24. Hu, X.; Wu, S.; Zhang, G.; Zheng, W.; Liu, C.; He, C.; Liu, Z.; Guo, X.; Zhang, H. Landslide displacement prediction using kinematics-based random forests method: A case study in Jinping Reservoir Area, China. *Eng. Geol.* **2021**, *283*, 105975. [[CrossRef](#)]
25. Wang, R.; Zhang, K.; Wang, W.; Meng, Y.; Yang, L.; Huan, H. Hydrodynamic landslide displacement prediction using combined extreme learning machine and random search support vector regression model. *Eur. J. Environ. Civ. Eng.* **2020**, *2020*, 2345–2357. [[CrossRef](#)]
26. Zhang, Y.; Tang, J.; He, Z.; Tan, J.; Li, C. A novel displacement prediction method using gated recurrent unit model with time series analysis in the Erdaohe landslide. *Nat. Hazards* **2021**, *105*, 783–813. [[CrossRef](#)]
27. Yang, B.; Yin, K.; Lacasse, S.; Liu, Z. Time series analysis and long short-term memory neural network to predict landslide displacement. *Landslides* **2019**, *16*, 677–694. [[CrossRef](#)]
28. Miao, F.; Wu, Y.; Xie, Y.; Li, Y. Prediction of landslide displacement with step-like behavior based on multialgorithm optimization and a support vector regression model. *Landslide* **2017**, *15*, 475–488. [[CrossRef](#)]
29. Liu, Z.; Guo, D.; Lacasse, S.; Li, J.; Yang, B.; Choi, J. Algorithms for intelligent prediction of landslide displacements. *J. Zhejiang Univ. Sci. A* **2020**, *21*, 412–429. [[CrossRef](#)]
30. Wang, Y.; Tang, H.; Huang, J.; Wen, T.; Ma, J.; Zhang, J. A comparative study of different machine learning methods for reservoir landslide displacement prediction. *Eng. Geol.* **2022**, *298*, 106544. [[CrossRef](#)]
31. Lin, Z.; Sun, X.; Ji, Y. Landslide Displacement Prediction Model Using Time Series Analysis Method and Modified LSTM Model. *Electronics* **2022**, *11*, 1519. [[CrossRef](#)]
32. Lin, Z.; Sun, X.; Ji, Y. Landslide Displacement Prediction based on Time Series Analysis and Double-BiLSTM Model. *Int. J. Environ. Res. Public Health* **2022**, *19*, 2077. [[CrossRef](#)]
33. Guo, Z.; Chen, L.; Gui, L.; Du, J.; Do, H.M. Landslide displacement prediction based on variational mode decomposition and WA-GWO-BP model. *Landslides* **2019**, *17*, 567–583. [[CrossRef](#)]
34. Liu, Q.; Lu, G.; Dong, J. Prediction of landslide displacement with step-like curve using variational mode decomposition and periodic neural network. *Bull. Eng. Geol. Environ.* **2021**, *80*, 3783–3799. [[CrossRef](#)]
35. Xu, S.; Niu, R. Displacement prediction of Baijiabao landslide based on empirical modedecomposition and long short-term memory neural network in Three Gorgesarea, China. *Comput. Geosci.* **2018**, *111*, 87–96. [[CrossRef](#)]
36. Cai, Z.; Xu, W.; Meng, Y.; Chong, S.; Wang, R. Prediction of landslide displacement based on GA-LSSVM with multiple factors. *Bull. Eng. Geol. Environ.* **2015**, *75*, 637–646. [[CrossRef](#)]

37. Zhou, C.; Yin, K.; Ying, C.; Emanuele, I.; Bayes, A.; Filippo, C. Displacement prediction of step-likelandslide by applying a novel kernel extreme learning machine method. *Landslides* **2018**, *15*, 2211–2225. [[CrossRef](#)]
38. Huang, F.; Yin, K.; Zhang, G.; Gui, L.; Yang, B.; Liu, L. Landslide displacement prediction using discrete wavelet transform and extreme learning machine based on chaos theory. *Environ. Earth Sci.* **2016**, *75*, 1376. [[CrossRef](#)]
39. Yi, W.; Chuannuo, X.; Yu, W.; Cheng, X. A comprehensive diagnosis method of rolling bearing fault based on CEEMDAN-DFA-improved wavelet threshold function and QPSO-MPE-SVM. *Entropy* **2021**, *23*, 1142.
40. Peterson, O.J.; Siaw, F.; Anokye, M.A.; Samuei, A.; Emmaniel, N.G.; Prof, D.A.; George, T. COVID-19 as Information Transmitter to Global Equity Markets: Evidence from CEEMDAN-Based Transfer Entropy Approach. *Math. Probl. Eng.* **2021**, *2021*, 8258778.
41. Cem, E.; Mustafa, T. Wind speed estimation using novelty hybrid adaptive estimation model based on decomposition and deep learning methods (ICEEMDAN-CNN). *Energy* **2022**, *249*, 123785.
42. Vishnu, P.M.; Anil, K.B.; Srinivasa, R.S. Grey Relational Analysis-Based Objective Function Optimization for Predictive Torque Control of Induction Machine. *IEEE Trans. Ind. Appl.* **2020**, *57*, 835–844.
43. Arash, K.; Ali, P.; Ali, S.; Tao, M. Optimization of a novel photovoltaic thermal module in series with a solar collector using Taguchi based grey relational analysis. *Sol. Energy* **2021**, *215*, 492–507.
44. Senthilkumar, S.; Karthick, A.; Madavan, R.; Moshi AA, M.; Bharathi, S.S.; Saroja, S.; Dhanalakshmi, C.S. Optimization of Transformer Oil blended with Natural Ester Oils using Taguchi-based Grey Relational Analysis. *Fuel* **2021**, *288*, 119629. [[CrossRef](#)]
45. Reshef, D.N.; Reshef, Y.; Grossman, S.R.; Lander, E.S.; Finucane, H.K.; McVean, G.; Turnbaugh, P.J.; Mitzenmacher, M.; Sabeti, P.C. Detecting novel associations in large data sets. *Science* **2011**, *334*, 1518–1524. [[CrossRef](#)]
46. Yalan, J.; Chaoshun, L.; Zhixin, Y.; Yujie, Z.; Xianbo, W. Remaining Useful Life Estimation Combining Two-Step Maximal Information Coefficient and Temporal Convolutional Network With Attention Mechanism. *IEEE Access.* **2021**, *9*, 16323–16336.
47. Young, R.C.; Rhee, M.K. Face Video Retrieval Based on the Deep CNN With RBF Loss. *IEEE Trans. Image Process.* **2021**, *30*, 1015–1029.
48. Zian, L.; Ji, Y.; Liang, W.; Sun, X. Landslide Displacement Prediction Based on Time-Frequency Analysis and LMD-BiLSTM Model. *Mathematics* **2022**, *10*, 2203.
49. Yujie, F.; Jian, L.; Yang, L.; Suge, W.; Deyu, L.; Xiaoli, L. Multiple Perspective Attention Based on Double BiLSTM for Aspect and Sentiment Pair Extract. *Neurocomputing* **2021**, *438*, 302–311.
50. Zhenzhu, M.; Jinxin, Z.; Yating, H.; Christophe, A. Temporal Prediction of Landslide-Generated Waves Using a Theoretical-Statistical Combined Method. *J. Mar. Sci. Eng.* **2023**, *11*, 1151.
51. Du, H.; Song, D.; Chen, Z.; Shu, H.; Guo, Z. Prediction model oriented for landslide displacement with step-like curve by applying ensemble empirical mode decomposition and the PSO-ELM method. *J. Clean. Prod.* **2020**, *270*, 122248. [[CrossRef](#)]
52. Zhen, G.; Bin, Y.; Mengyan, H.; Wensi, W.; Yu, J.; Fang, Z. A novel hybrid method for flight departure delay prediction using Random Forest Regression and Maximal Information Coefficient. *Aerosp. Sci. Technol.* **2021**, *116*, 106822.
53. Benyang, Z.; Wei, L.; Li, X.; Shiyu, L.; Yang, Z.; Huang, Y.; Zhou, M. A CNN-based FBG demodulation method adopting the GAF-assisted ascending dimension of complicated signal. *Opt. Commun.* **2021**, *499*, 127296.
54. Ningtao, C.; Dajing, C.; Bin, L.; Jing, F.; Hongyang, W. A biosensing method for the direct serological detection of liver diseases by integrating a SERS-based sensor and a CNN classifier. *Biosens. Bioelectron.* **2021**, *186*, 113246.
55. Yu, C.; Fang, R.; Liang, T.; Sha, Z.; Li, S.; Yi, Y.; Zhou, W.; Song, H. Stock Price Forecast Based on CNN-BiLSTM-ECA Model. *Sci. Program.* **2021**, *2021*, 2446543.
56. Mohammed, A.B.; Muhammad, Y.N.; Imad, E.A.; Shaharin, A.S. BiLSTM Network-Based Approach for Solar Irradiance Forecasting in Continental Climate Zones. *Energies* **2022**, *15*, 2226.
57. Devi, K.; Paulraj, D.; Muthusenthil, B. Deep Learning Based Security Model for Cloud based Task Scheduling. *KSII Trans. Internet Inf. Syst.* **2020**, *14*, 3663–3679.
58. Lian, C.; Zeng, Z.; Wang, X.; Yao, W.; Su, Y.; Tang, H. Landslide displacement interval prediction using lower upper bound estimation method with pre-trained random vector functional link network initialization. *Neural Netw.* **2020**, *130*, 286–296. [[CrossRef](#)]
59. Xing, Y.; Yue, J.; Chen, C.; Qin, Y.; Hu, J. A hybrid prediction model of landslide displacement with risk-averse adaptation. *Comput. Geosci.* **2020**, *141*, 104527. [[CrossRef](#)]
60. Zhou, C.; Yin, K.; Cao, Y.; Ahmed, B. Application of time series analysis and PSO-SVM model in predicting the Bazimen landslide in the Three Gorges Reservoir, China. *Eng. Geol.* **2016**, *204*, 108–120. [[CrossRef](#)]
61. Huang, F.; Huang, J.; Jiang, S.; Zhou, C. Landslide displacement prediction based on multivariate chaotic model and extreme learning machine. *Eng. Geol.* **2017**, *218*, 173–186. [[CrossRef](#)]
62. Wang, Y.; Tang, H.; Wen, T.; Ma, J. A hybrid intelligent approach for constructing landslide displacement prediction intervals. *Appl. Soft Comput.* **2019**, *81*, 105506. [[CrossRef](#)]

Disclaimer/Publisher’s Note: The statements, opinions and data contained in all publications are solely those of the individual author(s) and contributor(s) and not of MDPI and/or the editor(s). MDPI and/or the editor(s) disclaim responsibility for any injury to people or property resulting from any ideas, methods, instructions or products referred to in the content.